Title:

Incorporation of water-derived hydrogen into methane during artificial maturation of kerogen under hydrothermal conditions

A manuscript prepared for submission to *Organic Geochemistry on* 25 June 2021

Authors and affiliations:

David T. Wang[a,b,c]*, Jeffrey S. Seewald[b], Eoghan P. Reeves[d], Shuhei Ono[a], and Sean P. Sylva[b]

[a]Department of Earth, Atmospheric and Planetary Sciences, Massachusetts Institute of Technology, Cambridge, Massachusetts 02139, USA.
[b]Marine Chemistry and Geochemistry Department, Woods Hole Oceanographic Institution, Woods Hole, Massachusetts 02543, USA.
[c]ExxonMobil Upstream Research Company, Spring, Texas 77389, USA.
[d]Department of Earth Science and Centre for Geobiology, University of Bergen, Bergen N-5020, Norway.

* Corresponding author at: Esso Exploration and Production Guyana Ltd, 86 Duke Street, Georgetown, Guyana.
E-mail address: dtw@alum.mit.edu or david.t.wang@exxonmobil.com (D.T. Wang).

Keywords:
methane, natural gas generation kinetics, D/H ratios, kerogen, clumped isotopologues, hydrogen isotope exchange, water isotopes

Abstract

To investigate the origin of H in thermogenic methane, a sample of organic-rich Eagle Ford shale was reacted with D_2O under hydrothermal conditions in a flexible Au-Ti cell hydrothermal apparatus in a water-to-rock ratio of approximately 5:1. Temperatures were increased from 200 to 350 °C over the course of one month, maintaining pressure at 350 bar, and the concentrations of aqueous species and methane isotopologues produced were quantified. Production of H_2, CO_2, alkanes, and alkenes was observed. Methane formed during the early stages of the experiment at 200 °C was primarily CH_4 with some CH_3D, whereas at higher temperatures, increasing proportions of deuterated isotopologues were produced. Near the end of the experiment, the concentration of CD_4 exceeded that of all other isotopologues combined. These results suggest that competition between rates of kerogen-water isotopic exchange and natural gas generation may govern the D/H ratio of thermogenic gases.

Abstract: 147 words

Main Text: XXXX words

1. INTRODUCTION

Variation in δD values of thermogenic natural gases is often attributed to kinetically-controlled fractionation during pyrolysis of kerogen or oils. A number of studies have investigated how D/H ratios of methane and other hydrocarbons evolve with increasing maturity (Sackett, 1978; Berner et al., 1995; Sackett and Conkright, 1997; Tang et al., 2005; Ni et al., 2011). However, kinetic isotope effects involving hydrogen addition or abstraction are often large and by themselves do not explain the geologically-reasonable apparent equilibrium temperatures of ~150 to 220 °C obtained for reservoir gases that have been studied for their clumped isotopologue compositions (Stolper et al., 2014, 2015; Wang et al., 2015; Douglas et al., 2017; Young et al., 2017; Shuai et al., 2018; Giunta et al., 2019; Labidi et al., 2020; Thiagarajan et al., 2020). There is also evidence that δD values of CH_4 approach values expected for isotopic equilibrium between CH_4 and H_2O in formation waters at temperatures characterizing reservoirs and/or mature source rocks (~150 to 250 °C) (Clayton, 2003; Wang et al., 2015), although findings of insignificant hydrogen exchange occurring under these conditions also exist (Yeh and Epstein, 1981). In order for methane samples to have approached or attained equilibrium values of $\Delta^{13}CH_3D$ and $\Delta^{12}CH_2D_2$—parameters that describe the abundance of clumped isotopologues relative to a population of molecules containing isotopes randomly distributed amongst them [e.g., Young et al. (2017)]—there must be a pathway by which either (*i*) isotopes can be exchanged amongst methane isotopologues alone, (*ii*) methane isotopologues exchange hydrogen with water or organic molecules, or (*iii*) methane isotopologues are derived from methyl moieties which contain C–H bonds that have pre-exchanged with water prior to forming methane (Hoering, 1984; Smith et al., 1985; Schimmelmann et al., 1999, 2006; Lis et al., 2006).

Here, we study the origin of C–H bonds in thermogenic methane by heating kerogen in the presence of D_2O and examining the degree of deuteration in the generated methane. This experiment is conceptually very similar to those conducted by Hoering (1984), Lewan (1997), and Schimmelmann et al. (2001). However, none of these workers quantified the extent of deuteration in the produced natural gases, though Lewan mentioned that methane formed in his experiments contained deuterium [Lewan (1997) and M. D. Lewan (pers. comm.)].

2. METHODS

2.1. Experimental methods

Experiments were conducted in a gold-titanium reaction cell housed within a flexible cell hydrothermal apparatus (Seyfried et al., 1987) at WHOI. The reaction cell was pre-treated prior to loading by soaking in concentrated HCl for 4 hours, followed by rinsing with water to pH neutral and drying in the oven. The exit tube of the apparatus was cleaned by forcing ~20 ml of MilliQ deionized water (18.2 MΩ) through, followed by ~20 ml conc. HCl, ~100 ml water, ~20 ml conc. HNO_3, and then ~100 ml of water until the pH tested 7 using pH paper.

The source material for this experiment was a hand sample of Upper Cretaceous Eagle Ford Shale taken from an outcrop in Uvalde County, Texas, USA (Hentz and Ruppel, 2010). The sample was kindly provided to J. Seewald by Keith F. M. Thompson (PetroSurveys, Inc.). There is no known oil or gas production from the Eagle Ford in Uvalde County [(Tian et al., 2013); and IHS (2019)]. The Eagle Ford here is thermally-immature [R_o = 0.40–0.55%, Cardneaux (2012); Cardneaux and Nunn (2013); and Harbor (2011)]. The sample was powdered to <250 μm and Soxhlet-extracted (by Carl Johnson, WHOI) to remove bitumen and free hydrocarbons. In a subsequent step, the solvent-extracted residue was subjected to hydrochloric acid treatment to remove carbonate minerals. Elemental

analysis (**Table 1**) of the original rock sample (UNEX), the Soxhlet-extracted rock sample (EX), and the decalcified+extracted rock sample (DECA) indicates a total organic carbon (TOC) content of ~2.5% and a carbonate content of ~80% by weight. The H/C atomic ratio of the decalcified rock is 2.4. This value is probably several tens of percent higher than the actual H/C ratio of isolated kerogen (not determined) given that substantial amounts of H are likely borne by clays and other minerals that were not removed (Whelan and Thompson-Rizer, 1993; Baskin, 1997). The reaction cell was loaded with 10.03 grams of the EX powder.

Geochemical data for the Eagle Ford sample can be drawn from neighboring Kinney County, Texas, where complete sections of immature Eagle Ford have been recovered by the USGS (drill core GC-3; French et al., 2020) and Shell (Iona-1 drill core; Eldrett et al., 2014, 2015; Sun et al., 2016); there, the Eagle Ford also crops out, is immature, and is presumed to be geochemically similar. The high calcium carbonate content and relatively lower organic enrichment is consistent with data from the Upper Eagle Ford in the Shell Iona-1 core from neighboring Kinney County, Texas (Eldrett et al., 2015).

The starting fluid was heavy water (D_2O, 99% purity, Cambridge Isotope Laboratories, Inc.) containing some NaCl (0.497 mol/kg). The added NaCl allows for detection of dilution of the fluid by deionized water from the pressure vessel in the case of a leak in the reaction cell. The reaction cell was loaded with 55.03 g of this starting fluid. The pressure vessel was sealed and the reaction brought to initial condition (200 °C, 350 bar) rapidly. Several milliliters of fluid were bled during heat-up to prevent overpressurization, leaving an estimated 52.6 g of fluid in the cell at the beginning of the experiment (**Table 2**).

2.2. Analytical methods

To monitor the fluid composition and the extent of deuteration, sample aliquots of fluid were withdrawn through the capillary exit tube into gastight glass/PTFE syringes. Immediately prior to a sampling event, a small amount (~0.5 g) of fluid was removed and discarded in order to flush the exit tube of any residues. The concentration of molecular hydrogen (H_2) was determined after headspace extraction using a gas chromatograph supplied with nitrogen carrier gas, and equipped with a molecular sieve 5Å column and thermal conductivity detector. Analytical reproducibility of H_2 data is ±10% or better (2σ). However, accuracy of reported concentrations is unknown, because the relative responses of H_2, HD, and D_2 (the latter likely to be the main form of molecular hydrogen) in the GC-TCD were not determined. Residual liquid after headspace extraction was diluted with MilliQ water and saved for analysis of major cations and anions, or stored with dichloromethane in the fridge in a screw capped vial for analysis of non-volatile organic compounds.

Concentrations of total dissolved inorganic carbon (ΣCO_2) and C_1 to C_6 alkanes and alkenes were determined using a purge-and-trap cryofocusing device coupled to a gas chromatograph equipped with a Porapak Q column and serially-connected thermal conductivity and flame ionization detectors. Analytical procedures were as described in Reeves et al. (2012). Analytical reproducibility on duplicate samples was ±5% or better (2σ). The C_5 and C_6 compounds could not be quantified accurately due to their semi-volatile nature; however, C_5 and C_6 were detected at all sampling points.

At each sampling, a separate ~1 to 2 ml aliquot was injected directly into a pre-weighed, evacuated serum vial capped with boiled blue butyl rubber stoppers, for analysis of the extent of deuteration of methane. A Hewlett-Packard (HP) 6890 gas chromatography-mass spectrometry (GC-MS) system equipped with a 5Å molecular sieve column (HP-PLOT 30 m × 0.32 mm × 12.0 μm) and HP 5973 mass selective detector was used to determine the amount of deuteration in CH_4. Ion currents were monitored at integral masses between *m*/*z* 10 and 50. Extracted ion

currents were quantified at *m*/*z* 14 through 20 for methane. Expected fragmentation patterns of the five methane-*d* isotopologues were determined by analysis of commercial synthetic standards (>98% purity, Cambridge Isotope Laboratories, Inc.).

3. RESULTS

3.1. Temperature and thermal maturity

Temperatures logged during the experiment are shown in **Fig. 1A**. A fluid sample was taken at the beginning and end of each temperature stage. One additional sample (#4) was drawn in the middle of the second temperature stage (300 °C).

Estimated thermal maturity as a function of time was calculated using EASY%Ro (Sweeney and Burnham, 1990), and is shown in **Fig. 1B**. Maturities encountered in the experiment spanned the entire range of the oil window (ca. 0.5% to 1.3% R_o-equivalent; Burnham, 2019).

3.2. Concentrations of aqueous species

3.2.1. Inorganic species

Measured concentrations of aqueous species are shown in **Fig. 2**. Concentrations of H_2 increased from undetectable (<10 μmol/kg) to up to 0.8 mmol/kg at the end of the experiment. Increasing concentrations of H_2 within temperature stages of the experiment suggests that generation of petroleum, as opposed to a mineral redox buffer, is influencing the H_2 concentration. H_2 increased much more slowly during the >300 °C stages compared to heating at 300 °C and below.

The concentration of ΣCO_2 increased during the early stages of the experiment, and leveled off at ~50 mmol/kg at 350 °C. The plateauing inorganic carbon concentration might indicate that carbonate reached saturation and began to precipitate (Seewald et al., 1998). Measurements of major cations may be used to validate this interpretation. Production of CO_2 as the most abundant product of hydrothermal alteration of kerogen is also consistent with prior experimental work (Seewald, 2003). Alternatively, carbonate could have been released from the rock as it had not been decalcified prior to heating.

3.2.2. Alkanes and alkenes

Concentrations of methane increased in every successive time step, as did concentrations of detected *n*-alkanes. Except for the beginning of the experiment, molar concentrations of C_1 and ΣC_{2-4} were very similar and increased in near lock step.

Alkenes (ethylene and propylene, **Fig. 2D–E**) rose in concentration with every increase in temperature, indicating generation of unsaturated hydrocarbons via thermolytic processes. While concentrations of *n*-alkanes increased monotonically from the beginning to end of each temperature stage, the concentrations of alkenes were flat—or in the 350 °C stage, trended downwards—with time during each stage. Concentrations of alkenes consistent with thermodynamic equilibrium at measured H_2 concentrations are on the order of ~$10^{-7.3}$ and ~$10^{-6.5}$ mol/kg for ethylene and propylene, respectively, at 350 °C (Reeves et al., 2012). These equilibrium concentrations are ~2 orders of magnitude lower than the observed alkene concentrations.

Evidence from hydrothermal experiments suggests that metastable alkane/alkene equilibrium should be attained under hydrothermal conditions with half-equilibration times of several hundred hours or less at temperatures of 325 to 350 °C (Seewald, 1994). Failure to achieve thermodynamic equilibrium within these timescales indicates that generation of thermogenic alkenes occurs concurrently with alkane/alkene hydrogen exchange. Various pyrolysis experiments have reported alkene production (Huizinga et al., 1987; Leif and Simoneit, 2000), lending further support to the hypothesis that continued production of alkenes competes with their conversion into alkanes via hydrogenation at these temperatures and timescales and under the redox conditions characterizing hydrothermal maturation of organic-rich mudrocks.

Unlike the C_{2+} alkanes, methane cannot dehydrogenate to form an alkene. Hence, hydrogen exchange of methane requires that the very stable C–H bond be broken. Under appropriate, generally water-absent conditions, methane exchanges hydrogen with certain catalytic materials such as γ-alumina at room temperature over hours to days (Sattler, 2018, and refs. therein) [or with organometallic catalysts under even colder conditions (Golden et al., 2001)]. However, such catalysts in their active forms are not known to occur naturally in aqueous environments. Experiments conducted with aqueous methane in the presence of iron-bearing minerals reveal little-to-no observable exchange even over several months at temperatures as high as 323 °C (Reeves et al., 2012). Therefore, it is likely that hydrogen exchange of methane during the experiment was limited or insignificant, and that the hydrogen isotopic composition of the generated CH_4 is controlled primarily by the processes of source rock-water hydrogen exchange and kinetic isotope fractionation during methane generation. As discussed in the following section, this conclusion is supported by the selective production of deuterated methane isotopologues.

3.3. Production of deuterated methane isotopologues

Mass spectra collected for standards are shown in **Fig. 4**. Fragment intensities were very similar to those determined by Dibeler and Mohler (1950). Mass spectra of samples are shown in **Fig. 3**. No methane peaks of usable size could be obtained for time point #1. All other time points yielded quantifiable extracted ion chromatogram peaks.

The mass spectra of commercial standards were used to fit the sample data using a constrained linear least-squares solver (LSQNONNEG) implemented in MATLAB. Estimated relative abundances of methane-*d* isotopologues are shown in **Fig. 5A**.[1] Relative abundances were converted into absolute abundances (**Fig. 5B**) by multiplying by the methane concentration. The proportion of D in methane-bound hydrogen, calculated from the isotopologue abundances, is shown in **Fig. 6**.

Methane formed during the early stages of the experiment at 200 °C was primarily CH_4 with some CH_3D, whereas at higher temperatures, the isotopologues produced consist almost exclusively of CD_4, CHD_3, and CH_3D (**Fig. 5A** and **Fig. 6**). These results suggest that at relatively lower temperatures of ~200 °C, the rate of methane generation approaches or exceeds the rate of D/H exchange between water and kerogen, whereas at higher temperatures, extensive D/H exchange between kerogen (or oils, if they are also precursors of methane) and water occurs prior to methane generation. CD_4 became the dominant methane species at temperatures of 300 °C and above, suggesting that more than 50% of all labile, methane-generating sites on kerogen were fully deuterated. Alternatively, the dominance of CD_4 might be explained by direct CH_4–H_2O isotopic exchange occurring after the generation of primarily non-deuterated methane. This is unlikely given the sluggish pace at which D/H exchange occurs for methane

[1] Results of this experiment were first presented by one of us in a Ph.D. thesis (Wang, 2017). This earlier version incorrectly represented the relative concentrations of the isotopologues due to a mathematical error (neglected to divide by the relative peak areas of the pure isotopologue standards). As a result, Fig. B.3 of that thesis appears different than **Fig. 5** in this paper. This paper has the most correct version known to us.

(Reeves et al., 2012; Wang et al., 2018). Experiments in which normal water is heated in the presence of CD_4 while the D/H of water is monitored may yield a more sensitive determination of the rate of CH_4–H_2O exchange.

Production of CH_4 at the beginning of the experiment (indicates that the "capping" hydrogen was derived from kerogen or other H-containing species in the rock as opposed to water. Alternatively, the CH_4 observed at the first time point may have been sorbed to a solid phase and leached into the fluid. Production of CH_4 and CH_3D appeared to cease by midway through the 300 °C stage (time point #4, 284 hours). Continued (though relatively minor) production of methane that was not fully-deuterated (CHD_3 and CH_3D, **Fig. 5B**) suggests that kerogen or oil from which methane was generated did not fully exchange before methane formed.

If significant exchange were to occur, either between water and kerogen, or between water and generated methane after cracking, and this exchange occurs sequentially, the predominant isotopologue would be expected to follow the progression $CH_4 \rightarrow CH_3D \rightarrow CH_2D_2 \rightarrow CHD_3 \rightarrow CD_4$. Instead, CH_2D_2 represents a smaller fraction of the methane isotopologues than either CH_3D or CHD_3 at all times, and calculated proportions of CH_2D_2 do not exceed 10% at any point in the experiment (**Fig. 5A**). A possible explanation is that various CH_x moieties (e.g., aromatic C vs. methylene C vs. heteroatom-bound C) may have significantly different propensities to exchange and hydrogenation (cracking). Cracking that occurs much faster or slower than exchange may yield either fully-deuterated kerogen (e.g., $–CD_3$) or singly-deuterated methane, respectively, hence leading to an absence of CH_2D_2. Alternatively or additionally, D/H exchange of partially-deuterated longer-chain hydrocarbon molecules with water may be faster than cracking, such that the production of CH_2D_2 is "skipped". The absence of CH_2D_2 is additional evidence that exchange between water and methane or methane and methane at temperatures of 200 to 350 °C is slow on the timescales relevant to these experiments, consistent with a prior set of experiments (Reeves et al., 2012). Rates of methane isotopic exchange could potentially be better constrained by heating normal water in the presence of CD_4 and monitoring the rate of increase in the δD value of water.

CD_4 predominates towards the end of the experiment (from time point #7 onwards). This coincides with the end of the oil window (EASY%Ro between 0.9 and 1.3%) (**Fig. 6A**).

Fig. 6A shows the percentage of water-derived hydrogen in CH_4 vs. estimated maturity (EASY%Ro). Small symbols are from Wei et al. (2019). Some difference is expected given the different source rocks, experimental conditions, and that the aqueous media in HIPPIE-DIPPIE was D_2O instead of normal water. **Fig. 6B** is a graph of cumulative CH_4 generated plotted against percentage of methane deuteration.[2]

4. DISCUSSION

4.1. Interpretation of D/H and clumped isotope signatures of CH_4

4.2. Generation potential of natural gas

Asdfasfdasdf

[2] Calculated as $[CH_4] \times V_{remaining} + \sum([CH_4] + V_{withdrawn})$. Note that this doesn't account for any cracking of C_2 to C_5 compounds to CH_4.

4.3. BLAH BLAH BLAH BLAH

No longer limited by HI ….. can make as much as TOC allows (viz. Helgeson paper).

Other factors such as water pressure, fluid chemistry, fluid flow, the presence of oil or Type I organic matter and methane or CO2 partial pressures were found to play only minor roles in the development of vitrinite reflectance. (Huang 1996, exxon).

The literature is conflicted on the importance of water on vitrinite reflectance. For a review of the literature see Hackley and Lewan, 2018.

We compared several different models of vitrinite reflectance: EASY%Ro (Sweeney & Burnham, 1990), EASY%RoB (Burnham 2019), EASY%RoV (Burnham 2019), and Basin%Ro (Nielsen et al., 2016). We show both F (fraction of oil generated as mod-eled) and modeled %Ro (Fig. S-1A, S-1B).

We assumed here that parimary oil generation occurs principally within the range 0.5 to 1.3 %Ro-equivalent (Burnham, 2019). Under conditions encountered in this experiment, the modeled conversion of oil is between 5% and 95%, respectively (Fig. S1).

Zhang et al

Oil cracking hydrous: Jin et al, He et al 2019

Kerogen maturation hydrous: Gao et al., 2014 (higher maturity)

French et al, Eagle Ford geochemistry for Sorg/TOC

While Lewan (1997) did not quantify the abundance of deuterated methane isotopologues, we understand that these analyses have been conducted in follow-up. The data also show production of deuterated and perdeuterated isotopologues of methane (M.D. Lewan, personal correspondence).

While examining the total ion and extracted ion chromatograms to quantify the deuteration in CH_4, an unknown and unexpected peak was found eluting immediately following the CH_4 and air peaks. This mystery peak appeared to yield methyl fragments that were also progressively more deuterated with reaction time. Re-analysis of several samples while scanning a higher mass range suggested that the mystery compound had stable fragments near m/z 45 to 50 (depending on degree of deuterium substitution). This was verified by GC-MS analysis of a commercial isobutane standard (mostly isobutane-d_0) which yielded a base peak at m/z 43. No attempt to quantify the degree of deuteration in isobutane was made.

Comments in Wei et al., 2019, Org Geochem

Aromatic Hydrogen Exchange in Petroleum Source Rocks

R. Alexander, R. I. Kagi, A. V. Larcher and G. W. Woodhouse

School of Applied Chemistry, Western Australian Institute of Technology, Kent Street, Bentley, 6102, Western Australia, Australia

5. CONCLUSIONS

Three features in the dataset are notable: (*i*) the predominance of CD_4 at the end of the experiment, coinciding with the late oil window; (*ii*) the lack of direct methane-water isotopic exchange even at 350 °C; and (*iii*) the near-absence of CH_2D_2 during the experiment. These observations suggest that while some $–CH_x$ moieties in kerogen or longer-chain hydrocarbons undergo exchange more readily than cracking, some other moieties or compound classes are much less prone to exchange.

Carefully-controlled, temperature-programmed hydrous deuteration (deuterous pyrolysis or deuterothermal pyrolysis) experiments on additional source rocks and kerogen types may reveal systematic differences in the kinetics of exchangability vs. hydrocarbon generation. Such experiments have the potential of improving prediction of generative yields and oil compositions in basins where timing and quality of hydrocarbon charge are key uncertainties.

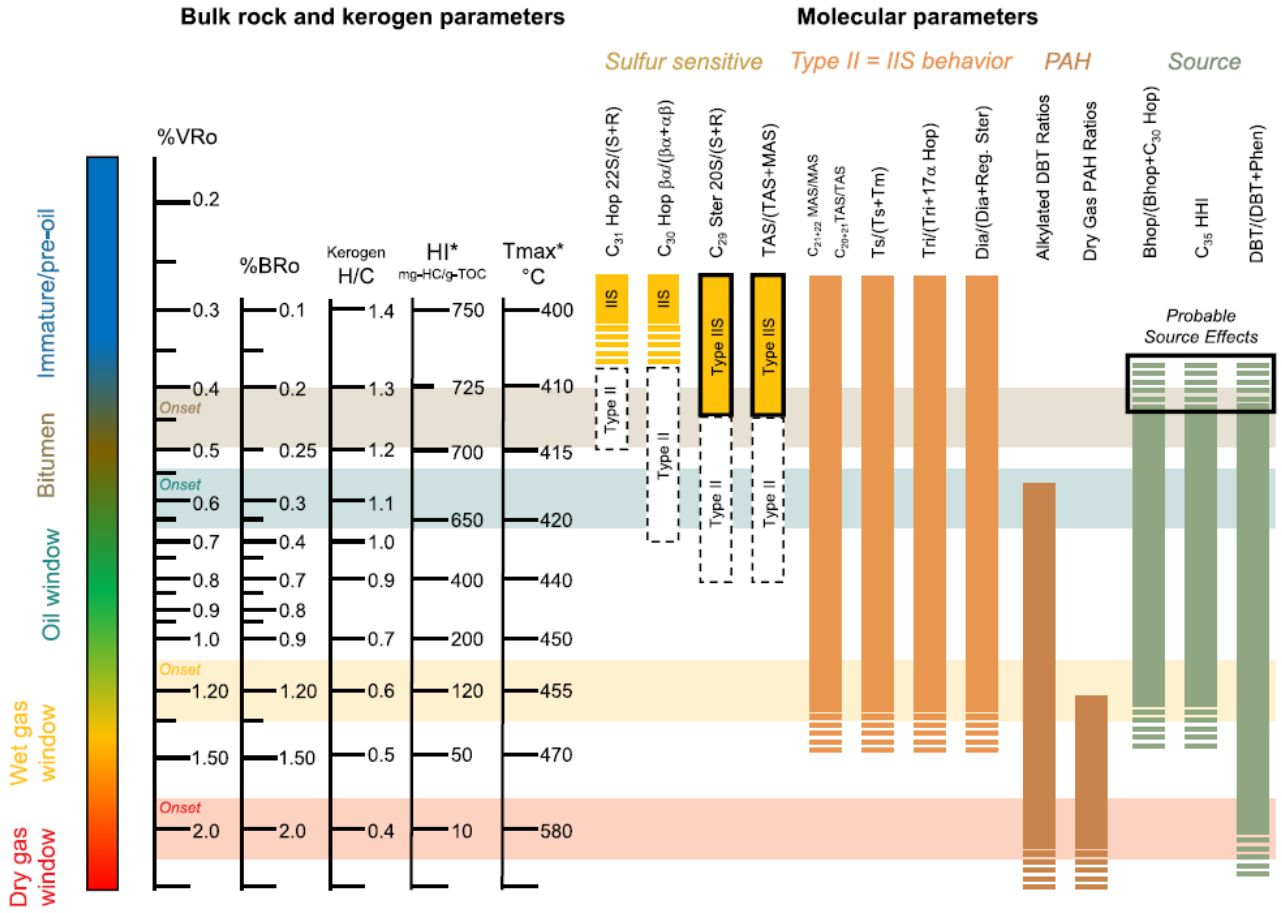

^ Oil window is 0.5 to 1.3 % Ro.

Thank you for giving me the link to your dissertation concerning clump isotopes of methane from various origins and settings. You did a fantastic job in interpreting, organizing and presenting the data on aqueous methane! I also enjoyed your pyrolysis work using the aqueous methane generated from the Eagle Ford sample.

The geochemistry that intrigues me is the reactions involving water dissolved in the bitumen of a source rock. Experiments indicate that the amount of water dissolved in the organic matter of a source rock determines the amount of oil expelled and retained in a maturing source rock. Understanding this aspect of dissolved water rather than aqueous organics is in its infancy, similar to that of the role of water dissolved in granite melts back in the 1930s. How does the amount of dissolved water and its chemistry influence the immiscibility of oil, hydrogen availability, and expulsion of oil from a source rock? Also, what reactions are occurring between dissolved water and bitumen to form H2 and CO2?

With respect to incorporating the role of water in numerical models there is a lot of work to be undertaken, but a Ph.D dissertation at Colorado School of Mines by Mohammed Al Duhailan (now with Saudi Aramco) has made

some preliminary quantitative attempts (attached). We have been doing some work on the effects of water on the mechanical properties of source rocks (attached). These studies are still rather qualitative but we are moving toward a more quantitative understanding. I put more emphasis on experimentation before numerical modeling is attempted.

6. ACKNOWLEDGMENTS

Financial support from the U.S. National Science Foundation (NSF awards EAR-1250394 to S.O., and XXX to J.S.S.), the Alfred P. Sloan Foundation via the Deep Carbon Observatory (to S.O. and J.S.S.), a Shell-MIT Energy Initiative Fellowship, and the Kerr-McGee Professorship at MIT (to S.O.) is acknowledged. We thank Aaron Sattler (ExxonMobil Research and Engineering) for advice on inverting mass spectral data, Keith F.M. Thompson for providing the Eagle Ford rock sample, and Chris Clayton for an email exchange that inspired this work. Comments by Michael Lewan on an earlier draft of this paper are gratefully acknowledged.

Potential reviewers: Katherine L. French, Justin Birdwell, Arndt Schimmelmann, Alex Sessions, Michael Lewan

Conflicted: John Eiler, Dan Stolper, Ed Young

7. REFERENCES

Baskin, D.K., 1997. Atomic H/C ratio of kerogen as an estimate of thermal maturity and organic matter conversion. AAPG bulletin 81, 1437–1450.

Berner, U., Faber, E., Scheeder, G., Panten, D., 1995. Primary cracking of algal and landplant kerogens: kinetic models of isotope variations in methane, ethane and propane. Chemical Geology 126, 233–245.

Burnham, A.K., 2019. Kinetic models of vitrinite, kerogen, and bitumen reflectance. Organic Geochemistry 131, 50–59.

Cardneaux, A., Nunn, J.A., 2013. Estimates of maturation and TOC from log data in the Eagle Ford Shale, Maverick Basin of South Texas. Gulf Coast Association of Geological Societies Transactions 63, 111–124.

Cardneaux, A.P., 2012. Mapping of the oil window in the Eagle Ford shale play of southwest Texas using thermal modeling and log overlay analysis (Masters Thesis). Louisiana State University.

Clayton, C., 2003. Hydrogen isotope systematics of thermally generated natural gas. International Meeting on Organic Geochemistry, 21st, Kraków, Poland, Book Abstr. Part I 51–52.

Dibeler, V.H., Mohler, F.L., 1950. Mass spectra of the deuteromethanes. J. Research Nat. Bur. Standards 45, 441–444.

Douglas, P.M., Stolper, D.A., Eiler, J.M., Sessions, A.L., Lawson, M., Shuai, Y., Bishop, A., Podlaha, O.G., Ferreira, A.A., Neto, E.V.S., others, 2017. Methane clumped isotopes: Progress and potential for a new isotopic tracer. Organic Geochemistry 113, 262–282.

Eldrett, J.S., Ma, C., Bergman, S.C., Lutz, B., Gregory, F.J., Dodsworth, P., Phipps, M., Hardas, P., Minisini, D., Ozkan, A., Ramezani, J., Bowring, S.A., Kamo, S.L., Ferguson, K., Macaulay, C., Kelly, A.E., 2015. An astronomically calibrated stratigraphy of the Cenomanian, Turonian and earliest Coniacian from the Cretaceous Western Interior Seaway, USA: Implications for global chronostratigraphy. Cretaceous Research 56, 316–344.

Eldrett, J.S., Minisini, D., Bergman, S.C., 2014. Decoupling of the carbon cycle during Ocean Anoxic Event 2. Geology 42, 567–570.

French, K.L., Birdwell, J.E., Lewan, M.D., 2020. Trends in thermal maturity indicators for the organic sulfur-rich Eagle Ford Shale. Marine and Petroleum Geology 118, 104459.

Giunta, T., Young, E.D., Warr, O., Kohl, I., Ash, J.L., Martini, A., Mundle, S.O., Rumble, D., Pérez-Rodríguez, I., Wasley, M., others, 2019. Methane sources and sinks in continental sedimentary systems: New insights from paired clumped isotopologues 13CH3D and 12CH2D2. Geochimica et Cosmochimica Acta 245, 327–351.

Golden, J.T., Andersen, R.A., Bergman, R.G., 2001. Exceptionally low-temperature carbon–hydrogen/carbon–deuterium exchange reactions of organic and organometallic compounds catalyzed by the $Cp^*(PMe_3)IrH(ClCH_2Cl)^+$ cation. Journal of the American Chemical Society 123, 5837–5838.

Harbor, R.L., 2011. Facies characterization and stratigraphic architecture of organic-rich mudrocks, Upper Cretaceous Eagle Ford Formation, South Texas (Masters Thesis). University of Texas at Austin.

Hentz, T.F., Ruppel, S.C., 2010. Regional lithostratigraphy of the Eagle Ford Shale: Maverick Basin to East Texas Basin. Gulf Coast Association of Geological Societies Transactions 60, 325–337.

Hoering, T., 1984. Thermal reactions of kerogen with added water, heavy water and pure organic substances. Organic Geochemistry 5, 267–278.

Huizinga, B.J., Tannenbaum, E., Kaplan, I.R., 1987. The role of minerals in the thermal alteration of organic matter—IV. Generation of n-alkanes, acyclic isoprenoids, and alkenes in laboratory experiments. Geochimica et Cosmochimica Acta 51, 1083–1097.

Hunt, J.M., 1996. Petroleum geochemistry and geology, 2nd ed.

IHS Markit Well Database, 2019.

Labidi, J., Young, E.D., Giunta, T., Kohl, I.E., Seewald, J., Tang, H., Lilley, M.D., Früh-Green, G.L., 2020. Methane thermometry in deep-sea hydrothermal systems: Evidence for re-ordering of doubly-substituted isotopologues during fluid cooling. Geochimica et Cosmochimica Acta 288, 248–261.

Leif, R.N., Simoneit, B.R., 2000. The role of alkenes produced during hydrous pyrolysis of a shale. Organic Geochemistry 31, 1189–1208.

Lewan, M., 1997. Experiments on the role of water in petroleum formation. Geochimica et Cosmochimica Acta 61, 3691–3723.
Lis, G.P., Schimmelmann, A., Mastalerz, M., 2006. D/H ratios and hydrogen exchangeability of type-II kerogens with increasing thermal maturity. Organic Geochemistry 37, 342–353.
Ni, Y., Ma, Q., Ellis, G.S., Dai, J., Katz, B., Zhang, S., Tang, Y., 2011. Fundamental studies on kinetic isotope effect (KIE) of hydrogen isotope fractionation in natural gas systems. Geochimica et Cosmochimica Acta 75, 2696–2707.
Reeves, E.P., Seewald, J.S., Sylva, S.P., 2012. Hydrogen isotope exchange between \emphn-alkanes and water under hydrothermal conditions. Geochimica et Cosmochimica Acta 77, 582–599.
Sackett, W.M., 1978. Carbon and hydrogen isotope effects during the thermocatalytic production of hydrocarbons in laboratory simulation experiments. Geochimica et Cosmochimica Acta 42, 571–580.
Sackett, W.M., Conkright, M., 1997. Summary and re-evaluation of the high-temperature isotope geochemistry of methane. Geochimica et Cosmochimica Acta 61, 1941–1952.
Sattler, A., 2018. Hydrogen/Deuterium (H/D) exchange catalysis in alkanes. ACS Catalysis 8, 2296–2312.
Schimmelmann, A., Boudou, J.-P., Lewan, M.D., Wintsch, R.P., 2001. Experimental controls on D/H and \textsuperscript13C/\textsuperscript12C ratios of kerogen, bitumen and oil during hydrous pyrolysis. Organic Geochemistry 32, 1009–1018.
Schimmelmann, A., Lewan, M.D., Wintsch, R.P., 1999. D/H isotope ratios of kerogen, bitumen, oil, and water in hydrous pyrolysis of source rocks containing kerogen types I, II, IIS, and III. Geochimica et Cosmochimica Acta 63, 3751–3766.
Schimmelmann, A., Sessions, A.L., Mastalerz, M., 2006. Hydrogen isotopic (D/H) composition of organic matter during diagenesis and thermal maturation. Annual Review of Earth and Planetary Sciences 34, 501–533.
Seewald, J.S., 1994. Evidence for metastable equilibrium between hydrocarbons under hydrothermal conditions. Nature 370, 285–287.
Seewald, J.S., 2003. Organic–inorganic interactions in petroleum-producing sedimentary basins. Nature 426, 327–333.
Seewald, J.S., Benitez-Nelson, B.C., Whelan, J.K., 1998. Laboratory and theoretical constraints on the generation and composition of natural gas. Geochimica et Cosmochimica Acta 62, 1599–1617.
Seyfried, W.E., Jr., Janecky, D.R., Berndt, M.E., 1987. Rocking autoclaves for hydrothermal experiments, II. The flexible reaction-cell system. Hydrothermal Experimental Techniques 9, 216–239.
Shuai, Y., Etiope, G., Zhang, S., Douglas, P.M., Huang, L., Eiler, J.M., 2018. Methane clumped isotopes in the Songliao Basin (China): New insights into abiotic vs. biotic hydrocarbon formation. Earth and Planetary Science Letters 482, 213–221.
Smith, J., Rigby, D., Gould, K., Hart, G., Hargraves, A., 1985. An isotopic study of hydrocarbon generation processes. Organic Geochemistry 8, 341–347.
Stolper, D., Martini, A., Clog, M., Douglas, P., Shusta, S., Valentine, D., Sessions, A., Eiler, J., 2015. Distinguishing and understanding thermogenic and biogenic sources of methane using multiply substituted isotopologues. Geochimica et Cosmochimica Acta 161, 219–247.
Stolper, D.A., Lawson, M., Davis, C.L., Ferreira, A.A., Santos Neto, E.V., Ellis, G.S., Lewan, M.D., Martini, A.M., Tang, Y., Schoell, M., Sessions, A.L., Eiler, J.M., 2014. Formation temperatures of thermogenic and biogenic methane. Science 344, 1500–1503.
Sun, X., Zhang, T., Sun, Y., Milliken, K.L., Sun, D., 2016. Geochemical evidence of organic matter source input and depositional environments in the lower and upper Eagle Ford Formation, south Texas. Organic Geochemistry 98, 66–81.
Sweeney, J.J., Burnham, A.K., 1990. Evaluation of a Simple Model of Vitrinite Reflectance Based on Chemical Kinetics (1). AAPG Bulletin 74, 1559–1570.
Tang, Y., Huang, Y., Ellis, G.S., Wang, Y., Kralert, P.G., Gillaizeau, B., Ma, Q., Hwang, R., 2005. A kinetic model for thermally induced hydrogen and carbon isotope fractionation of individual *n*-alkanes in crude oil. Geochimica et Cosmochimica Acta 69, 4505–4520.

Thiagarajan, N., Xie, H., Ponton, C., Kitchen, N., Peterson, B., Lawson, M., Formolo, M., Xiao, Y., Eiler, J., 2020. Isotopic evidence for quasi-equilibrium chemistry in thermally mature natural gases. Proceedings of the National Academy of Sciences 117, 3989–3995.

Tian, Y., Ayers, W.B., McCain Jr, D., 2013. The Eagle Ford Shale play, south Texas: regional variations in fluid types, hydrocarbon production and reservoir properties, in: IPTC 2013: International Petroleum Technology Conference, European Association of Geoscientists & Engineers, p. IPTC 16808.

Wang, D.T., 2017. The geochemistry of methane isotopologues (PhD Thesis). Massachusetts Institute of Technology and Woods Hole Oceanographic Institution. doi:10.1575/1912/9052

Wang, D.T., Gruen, D.S., Lollar, B.S., Hinrichs, K.-U., Stewart, L.C., Holden, J.F., Hristov, A.N., Pohlman, J.W., Morrill, P.L., Könneke, M., Delwiche, K.B., Reeves, E.P., Sutcliffe, C.N., Ritter, D.J., Seewald, J.S., McIntosh, J.C., Hemond, H.F., Kubo, M.D., Cardace, D., Hoehler, T.M., Ono, S., 2015. Nonequilibrium clumped isotope signals in microbial methane. Science 348, 428–431.

Wang, D.T., Reeves, E.P., McDermott, J.M., Seewald, J.S., Ono, S., 2018. Clumped isotopologue constraints on the origin of methane at seafloor hot springs. Geochimica et Cosmochimica Acta 223, 141–158.

Wei, L., Gao, Z., Mastalerz, M., Schimmelmann, A., Gao, L., Wang, X., Liu, X., Wang, Y., Qiu, Z., 2019. Influence of water hydrogen on the hydrogen stable isotope ratio of methane at low versus high temperatures of methanogenesis. Organic Geochemistry 128, 137–147.

Whelan, J.K., Thompson-Rizer, C.L., 1993. Chemical Methods for Assessing Kerogen and Protokerogen Types and Maturity, in: Engel, M.H., Macko, S.A. (Eds.), Organic Geochemistry: Principles and Applications, Springer US, Boston, MA, p. 289–353.

Yeh, H.-W., Epstein, S., 1981. Hydrogen and carbon isotopes of petroleum and related organic matter. Geochimica et Cosmochimica Acta 45, 753–762.

Young, E.D., Kohl, I.E., Lollar, B.S., Etiope, G., Rumble, D., Li, S., Haghnegahdar, M.A., Schauble, E.A., McCain, K.A., Foustoukos, D.I., Sutclife, C., Warr, O., Ballentine, C.J., Onstott, T.C., Hosgormez, H., Neubeck, A., Marques, J.M., Pérez-Rodríguez, I., Rowe, A.R., LaRowe, D.E., Magnabosco, C., Yeung, L.Y., Ash, J.L., Bryndzia, L.T., 2017. The relative abundances of resolved $^{12}CH_2D_2$ and $^{13}CH_3D$ and mechanisms controlling isotopic bond ordering in abiotic and biotic methane gases. Geochimica et Cosmochimica Acta 203, 235–264.

8. FIGURES

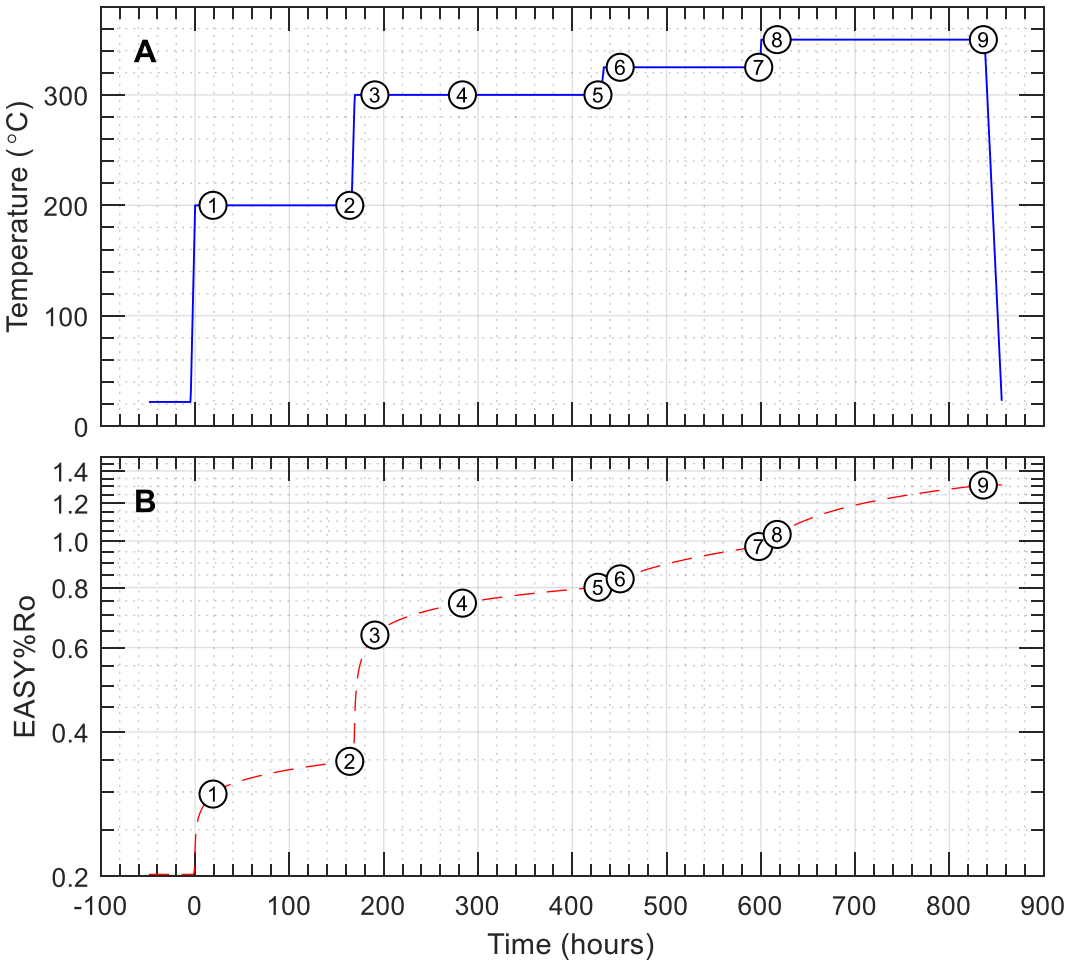

Fig. 1. Profiles of **(A)** temperature and **(B)** estimated maturity (as EASY%Ro) vs. time. Time-zero is the time at which the experiment was brought to initial conditions (200 °C and 350 bar). Numbers in circles represent sampling points (Table 2).

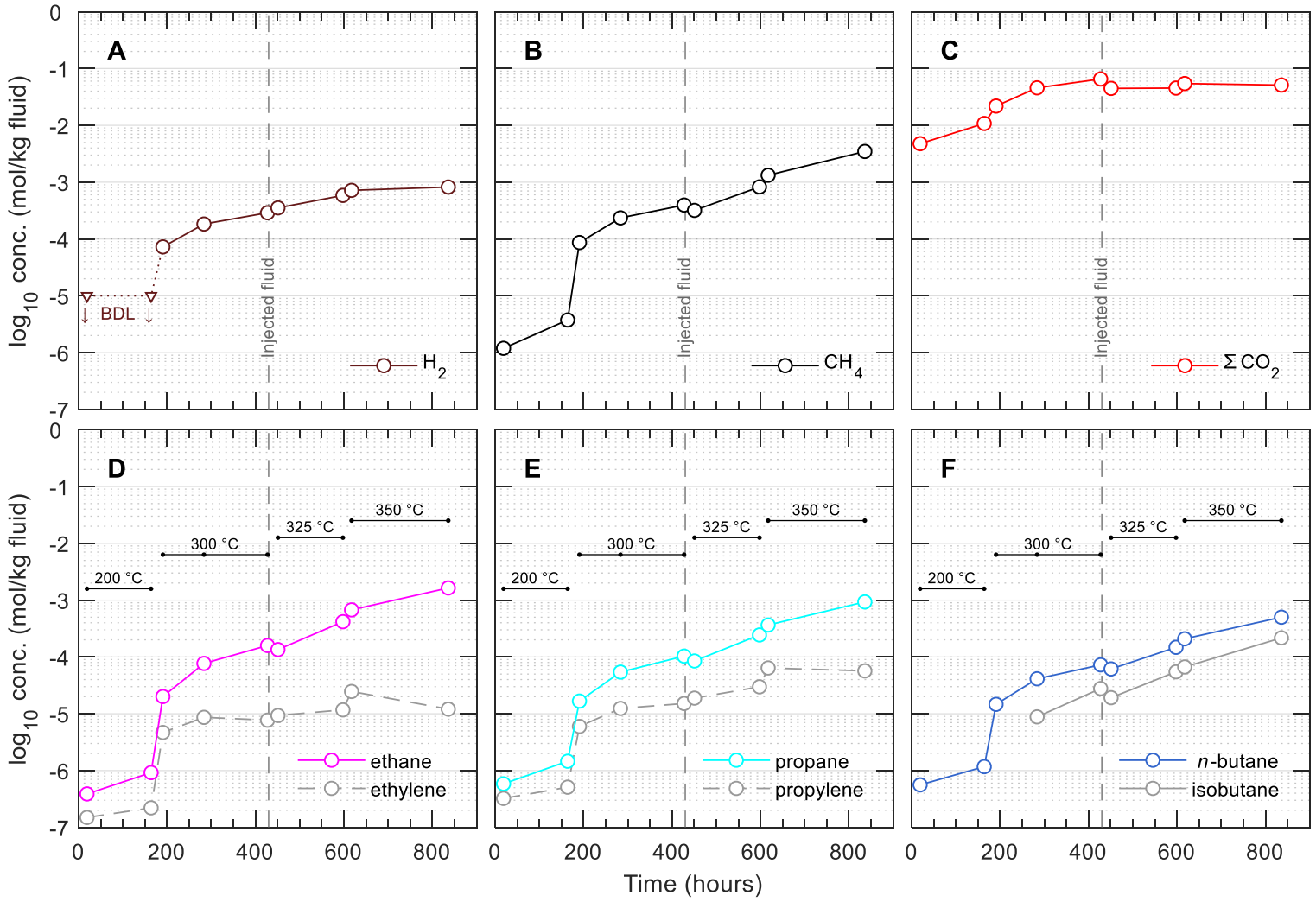

Fig. 2. Concentrations of aqueous species over time during the experiment. **(A)** Hydrogen (measured as H_2); **(B)** methane; **(C)** total inorganic carbon ($\sum CO_2$); **(D)** ethane and ethylene; **(E)** propane and propylene; and **(F)** *n*-butane and isobutane. Note that injection of additional saline D_2O at 430 hours diluted the concentration of all aqueous species by ~50%. BDL, below detection limit (<10 µmol/kg for H_2).

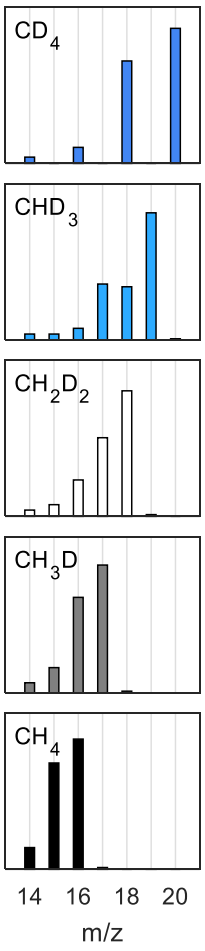

Fig. 3. Mass spectra of standards. Isotopologue is indicated in the upper left corner of each plot. Intensities were normalized such that the *m*/*z* 14 to 20 signals sum to unity.

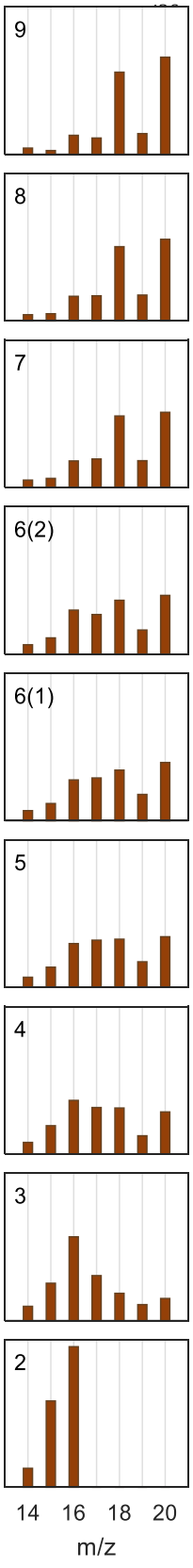

Fig. 4. Mass spectra of samples. Time point is indicated in the upper left corner of each plot. Intensities were normalized such that the *m*/*z* 14 to 20 signals sum to unity. Two samples were taken for time point #6, hence there are two plots.

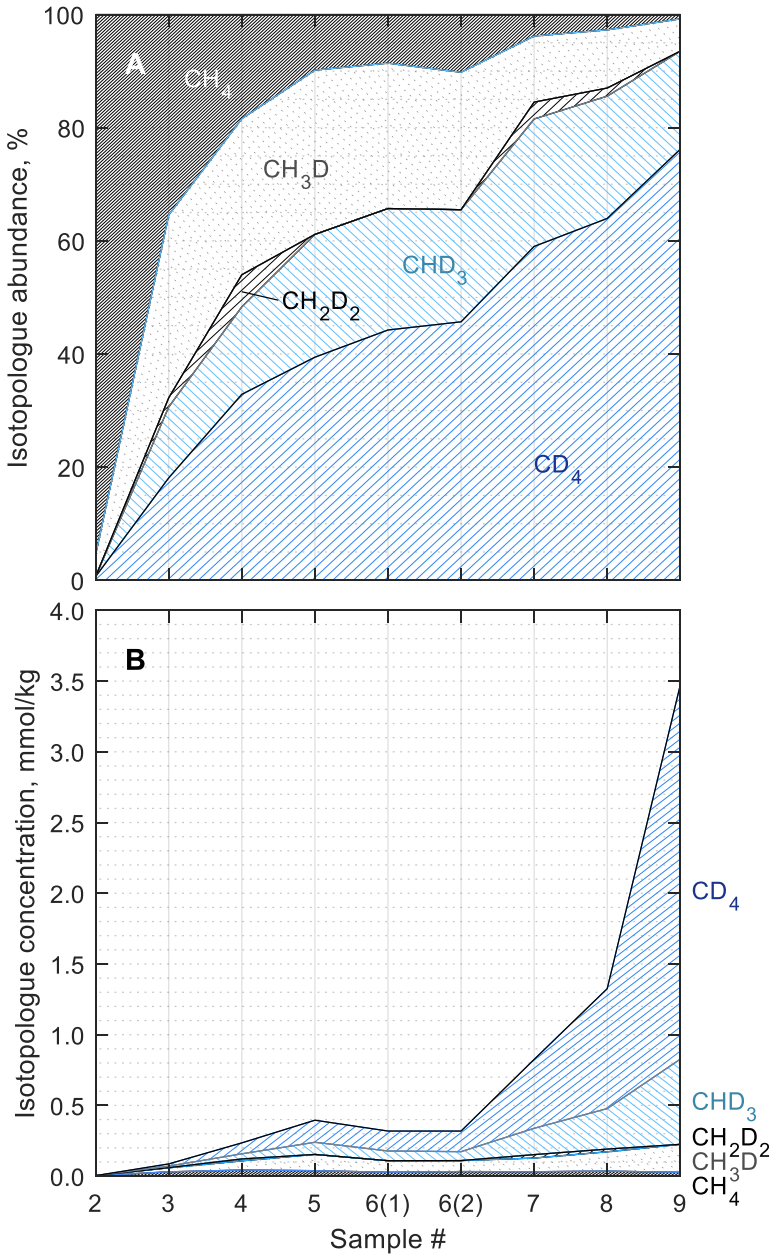

440

441 **Fig. 5.** Calculated **(A)** relative and **(B)** absolute abundances of methane isotopologues.

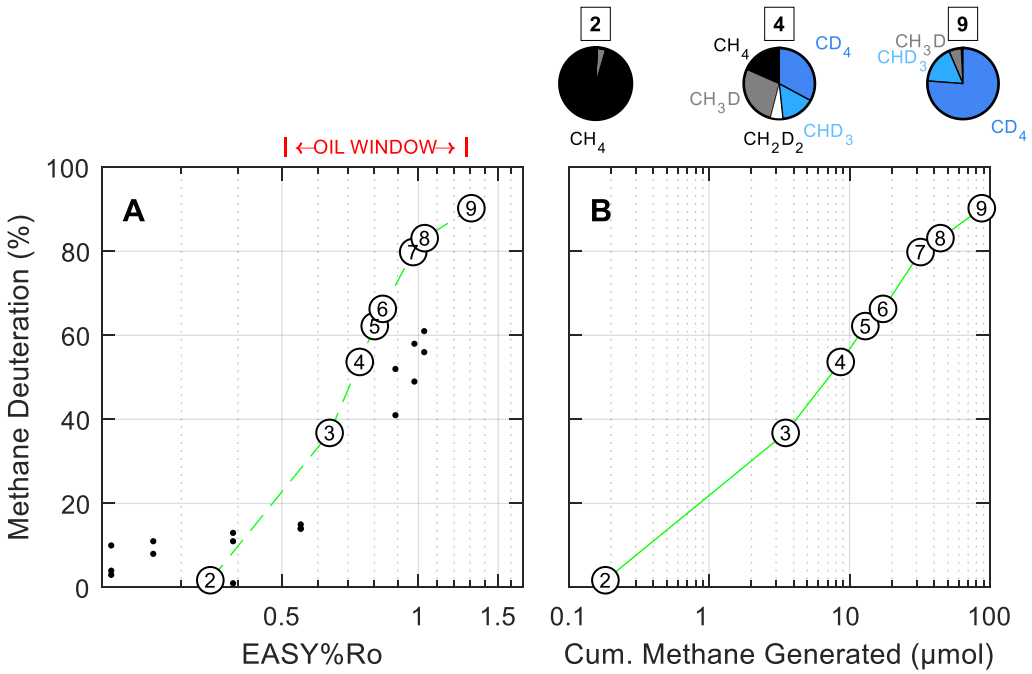

Fig. 6. Extent of methane deuteration [methane-bound D/(D+H)] vs. **(A)** estimated maturity (EASY%Ro) and **(B)** cumulative methane generated. The data shown for time point #6 is the average of the two replicate samples. Small symbols in (A) are data from Wei et al. (2019) representing percentage of water-derived H in CH_4 (see text). Pie charts above (B) represent relative abundances of isotopologues before, during, and after peak oil generation (time points #2, 4, and 9, respectively). Because approx.. 100 umol were generated, the bottom axis of B can be read as % of cumulative methane generation. It is seen that at 50% deuteration only less than 10% of methane has been generated; i.e., 90% of methane generated has more than 50% of its hydrogens coming from water. The volumetric significance of the water hydrogen reservoir hence may be more important than otherwise assumed. ***Is there HI vs. TOC vs. Ro data (or RockEval and TOC) data for global source rock databases? – ASK MIRELA, KIRSTEN, GRADY***

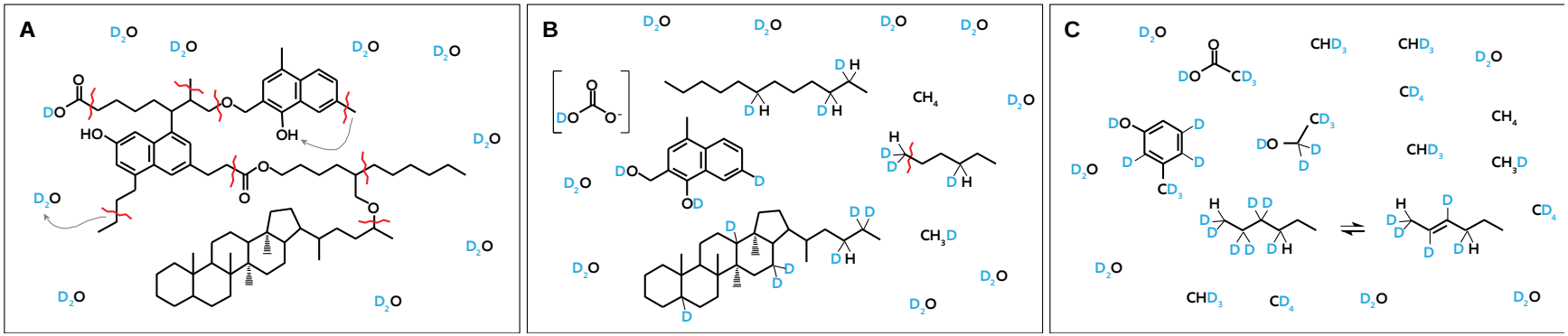

Fig. 7. Cartoon showing process of sequential deuteration of kerogen and oil along with generation of deuterated methane. Snapshots shown represent conditions of (A) mild heating (incipient catagenesis); (B) moderate heating (oil generation); and (C) extensive deuteration (gas window).

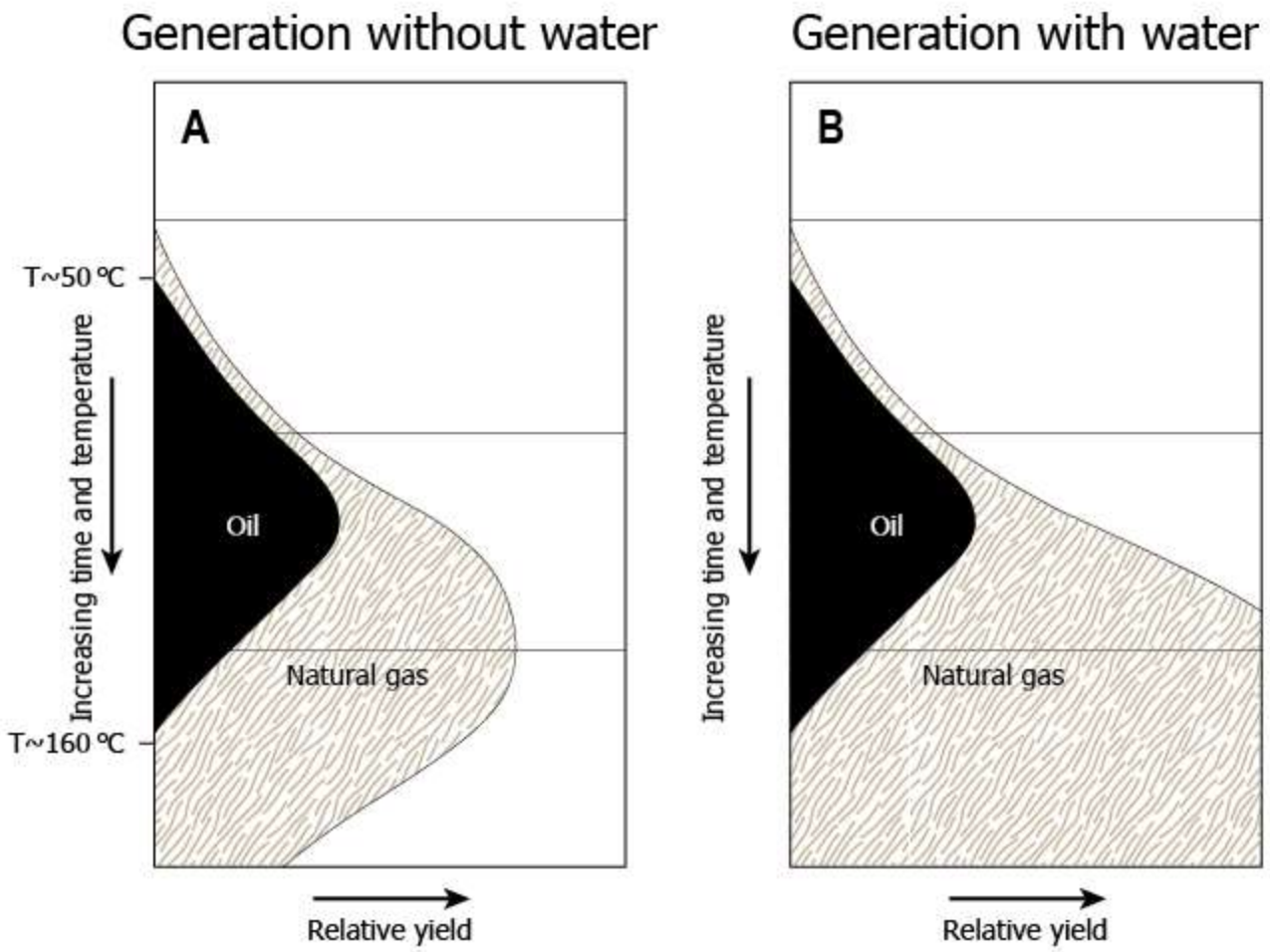

458

459 **Fig. 8.** Schematic yields of oil and natural gas when generation occurs from source rock in the absence (A) and
460 presence (B) of water as a source of hydrogen. (A) Traditional model of the amount and timing of organic altera-
461 tion products generated during progressive burial in sedimentary basins that assumes oxygen and hydrogen in or-
462 ganic alteration products are derived only from kerogen. The form of this figure is constrained by the maturation
463 trends shown in the Van Krevelen diagram. (B) Schematic illustration of the amount and timing of organic altera-
464 tion products generated if water and minerals are allowed to contribute the requisite hydrogen and oxygen for the
465 formation of hydrocarbons. Illustration is after Seewald (2003) and Hunt (1996).

466

TABLES

Table 1

Elemental analysis of Eagle Ford shale powder that was either: dried but otherwise untreated (UNEX), Soxhlet-extracted (EX), or extracted + decarbonated (DECA). Data from C. Johnson, WHOI, 1996.

(wt%)	UNEX	EX*	DECA
C	12.1	11.0	6.23
H	0.38	0.25	1.24
N	0.18	0.17	0.74
S	0.37	<0.2	2.3

*Used in the experiment.

Table 2

Concentration of aqueous species during heating of Soxhlet-extracted Eagle Ford shale at 200 to 350 °C and 350 bar in the presence of saline D_2O fluid.

Time Pt #	Time (h)	H_2 (µmol/kg)[a]	CH_4 (µmol/kg)	$\sum CO_2$ (mmol/kg)	$CH_4/\sum C_{2-4}$ [b]	$\sum H_2S$ (mmol/kg)	pD (25 °C)[c]
Experiment begun with 52.6 g of fluid at temperature of 200 °C							
1	19	BDL (<10)	1.2	4.8	0.78		
2	164	BDL (<10)	3.8	10.8	1.06		
Temperature raised to 300 °C							
3	191	773	8.7	21.9	1.68		
4	284	183	235	45.8	1.30		
5	427	290	396	65.5	1.09		
Injected ~18.3 g starting fluid and raised temperature to 325 °C							
6	451	353	319	44.7	1.06		
7	598	586	825	45.3	0.96		
Raised temperature to 350 °C							
8	617	718	1.32×10^3	54.4	1.01		
9	836	821	3.47×10^3	51.2	1.06	18.0	5.90

Analytical uncertainties (2*s*) are ±2 °C for *T*; ±5% for H_2, $\sum CO_2$, CH_4, and C_2 to C_4 hydrocarbons, ±2% for $\sum H_2S$; and ±0.05 units for pD. Concentrations are molar quantities per kg fluid.

[a] Determined from thermal conductivity response calibrated against a known H_2 standard. As discussed in the text, the listed hydrogen concentration was estimated as if all hydrogen were in the form of H_2. In reality, differences in the TCD response of H_2 and D_2 mean that the actual concentration of molecular hydrogen (likely primarily D_2) are somewhat different than those listed.

[b] Calculated as the molar ratio of methane to the sum of ethane, propane, isobutane, and *n*-butane.

[c] The listed pD value was calculated from pH measured with a glass electrode: $pD = pH_{measured} + 0.41$ (Glasoe and Long, 1960).